A PDMS-Based Conical-Well Microelectrode Array for Surface Stimulation and Recording of Neural Tissues

Liang Guo, *Student Member, IEEE*, Kathleen W. Meacham, *Student Member, IEEE*, Shawn Hochman, and Stephen P. DeWeerth*, *Senior Member, IEEE*

***Abstract*—A method for fabricating polydimethylsiloxane (PDMS) based microelectrode arrays (MEAs) featuring novel conical-well microelectrodes is described. The fabrication technique is reliable and efficient, and facilitates controllability over both the depth and the slope of the conical wells. Because of the high-PDMS elasticity (as compared to other MEA substrate materials), this type of compliant MEA is promising for acute and chronic implantation in applications that benefit from conformable device contact with biological tissue surfaces and from minimal tissue damage. The primary advantage of the conical-well microelectrodes—when compared to planar electrodes—is that they provide an improved contact on tissue surface, which potentially provides isolation of the electrode microenvironment for better electrical interfacing. The raised wells increase the uniformity of current density distributions at both the electrode and tissue surfaces, and they also protect the electrode material from mechanical damage (e.g., from rubbing against the tissue). Using this technique, electrodes have been fabricated with diameters as small as 10 μm and arrays have been fabricated with center-to-center electrode spacings of 60 μm. Experimental results are presented, describing electrode-profile characterization, electrode-impedance measurement, and MEA-performance evaluation on fiber bundle recruitment in spinal cord white matter.**

***Index Terms*—Compliant, conical-well microelectrode, conically recessed electrode, microelectrode array (MEA), microfabrication, neural prosthesis, polydimethylsiloxane (PDMS), surface recording, surface stimulation.**

I. Introduction

EXTRACELLULAR stimulation and recording of neuronal tissue have broad applicability both to scientific studies and to clinical applications. Historically, the majority of applications that elicit functional outputs have used single rigid electrodes inserted into the tissue [1], which provide local access to the targeted neurons. To improve resolution and reliability of both stimulation and recording, multiple-electrode approaches have been developed using semiconductor microfabrication techniques. These multielectrode arrays are typically fabricated using silicon, glass, and metals [2]–[7], and provide access to and control of proximal neural circuitry.

A significant limitation of these multielectrode approaches has been their mechanical impedance mismatch with surrounding tissue. This mismatch can lead to significant tissue damage and dysfunction of the device. Reduction of the multiple electrodes' invasiveness can be achieved by using planar multielectrode arrays that interface only with the tissue surface. This approach has worked effectively in applications, where reduced accessibility is an acceptable tradeoff. Rigid planar microelectrode arrays (MEAs) have been well developed and successfully applied in culture studies [8]–[12], but are still ultimately limited by their inability to interface closely with a soft-tissue substrate.

To improve the ability of multiple electrodes to interface closely and effectively with neural tissue surface, MEAs have been fabricated on flexible, thin-film substrates, such as polyimide [13]–[15]. These MEAs have been applied to many applications in biomedical engineering [13]–[20]. Although polyimide substrates exhibit a certain level of flexibility, they are not an ideal solution to the challenge of chronic surface stimulation and recording, primarily because the MEAs cannot conform to complex tissue surfaces. In contrast, MEAs fabricated using a truly compliant substrate, such as polydimethylsiloxane (PDMS, i.e., silicone rubber), have the capability of conforming to the tissue surface, which can provide a uniform and tight contact on the target tissue surface [21]–[23]. The combination of surface stimulation and recording with compliant MEAs provides a novel and potentially powerful method for exploring the underlying properties of the nervous system.

Building upon our previous PDMS-based MEA efforts [24], we have developed a new PDMS-based MEA fabrication method that features a conical PDMS well surrounding each microelectrode. These conical-well microelectrodes facilitate an improved tissue surface contact, which potentially provides a more isolated microenvironment for electrical current exchange between the electrode and tissue surface. In addition, this fabrication method is reliable and efficient with easy controllability over the conical well depth and recess slope. In this paper, we describe the fabrication processes, and we present experimental results for electrode-profile characterization, for electrode-impedance measurement, and for conical-well

Manuscript received January 24, 2010; revised April 21, 2010; accepted May 28, 2010. Date of publication June 14, 2010; date of current version September 15, 2010. This work was supported by the U.S. National Institutes of Health under Grant EB006179. *Asterisk indicates corresponding author.*

L. Guo and K. W. Meacham are with the Wallace H. Coulter Department of Biomedical Engineering, Georgia Institute of Technology, Atlanta, GA 30332 USA, and Emory University, Atlanta, GA 30332 USA (e-mail: liang.guo@gatech.edu; kwmeach@emory.edu).

S. Hochman is with the Department of Physiology, Emory University School of Medicine, Atlanta, GA 30322 USA (e-mail: shochm2@emory.edu).

*S. P. DeWeerth is with the Wallace H. Coulter Department of Biomedical Engineering, Georgia Institute of Technology, Atlanta, GA 30332 USA, and Emory University, Atlanta, GA 30332 USA (e-mail: steve.deweerth@gatech.edu).

Color versions of one or more of the figures in this paper are available online at http://ieeexplore.ieee.org.

Digital Object Identifier 10.1109/TBME.2010.2052617

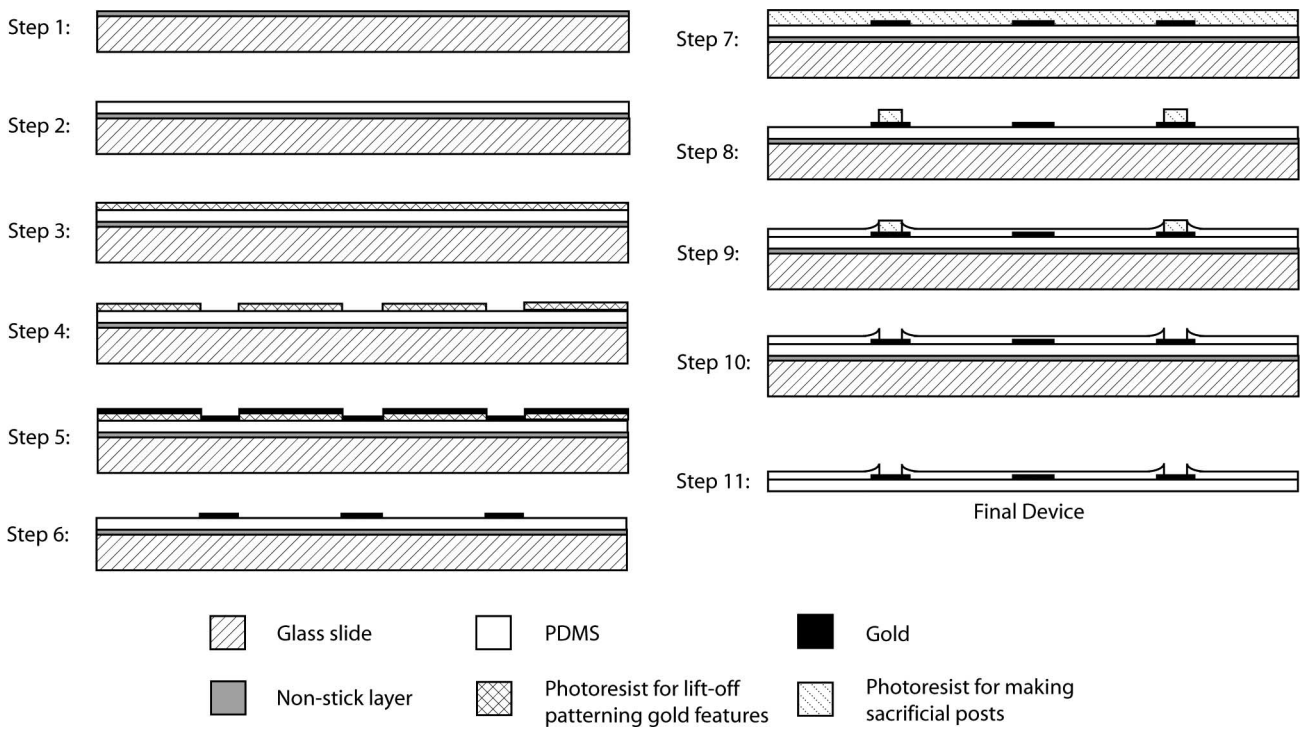

Fig. 1. Schematic illustration of stepwise fabrication processes for the PDMS-based conical-well MEA.

surface-contact testing. Finally, we evaluate MEA performance in the mammalian central nervous system via stimulation of spinal white matter tracts implicated in activating locomotor behavior.

II. Methodology

A. Device Fabrication

Briefly, our fabrication process involves curing a thin layer of PDMS onto a glass slide, liftoff patterning gold features, assisting in the formation of conical wells by lithographically defining sacrificial posts, where electrode and contact pad openings will be, covering the sample with another thinner PDMS layer for encapsulation, and then, removing the sacrificial posts to expose the electrodes and contact pads. Stepwise processes are shown schematically in Fig. 1 and are described in detail as following.

1) Preparing PDMS and Glass Slide: PDMS (Sylgard 184, Dow Corning) elastomer base is mixed with curing agent at 10:1 weight ratio, and the mixture is left at room temperature for at least 40 min to let air bubbles rise out. A cleaned glass slide is coated with a 250 Å nonstick gold layer primed by 100 Å titanium in an e-beam evaporator (CVC Products, Inc.), both at 3 Å/s, to facilitate device release in the end (Step 1 in Fig. 1). A $\sim$70-μm-PDMS base layer is formed by spin coating the prepolymer onto the glass slide at 1500 r/min for 15 s with a ramp rate of 1000 r/min/s. The sample is then cured on a hotplate (Step 2 in Fig. 1).

2) Liftoff Patterning Gold Traces: The sample is first briefly treated in oxygen plasma to activate the PDMS surface [25]. Immediately following this treatment, positive photoresist (Shipley Megaposit SPR 220 7.0) is spin coated at 1500 r/min for 30 s with a ramp rate of 300 r/min/s. The sample is then cured on a 90 °C hotplate with slow ramp up and down to avoid formation of cracks (Step 3 in Fig. 1). The resulting $\sim$12 μm photoresist is patterned in a standard photolithography process. Finally, the photoresist mask is flood-exposed to enable subsequent liftoff in its developer (Step 4 in Fig. 1). A hold time of at least 120 min is required before starting depositing gold to allow water, which is necessary to complete the photoreaction, to diffuse back into the photoresist mask. Then, 5000 Å gold is deposited at 1 Å/s in an e-beam evaporator with a priming layer of 300 Å titanium (Step 5 in Fig. 1). After deposition, the sample is soaked in the corresponding photoresist developer (Shipley Microposit MF-319) to dissolve the photoresist and liftoff the excess gold film, leaving only the desired gold features (Step 6 in Fig. 1).

3) Defining Sacrificial Posts: Following brief oxygen plasma treatment of the sample, a thick sacrificial layer of negative photoresist (NR5-8000, Futurrex, Inc., Franklin, NJ) is spin coated (Step 7 in Fig. 1). The sacrificial layer is patterned to leave posts right on top of each gold electrode and contact pad, where an opening is to be made (Step 8 in Fig. 1). The height of these sacrificial posts determines the depth of the conical electrode wells that will form [see Fig. 3(b)]. The processing recipe follows the NR5-8000 product data sheet, except that 90 °C is used during both softbake (60 min) and postbake (15 min) to avoid cracking gold features by high temperature.

4) Spin-Coating PDMS for Encapsulation: Immediately following oxygen plasma treatment, a second PDMS layer is spin coated to encapsulate the device at 5000 r/min for 150 s with a ramp rate of 1000 r/min/s. The uncured sample is left at room temperature for one hour, baked on a 60 °C hotplate for one hour, and then, baked in a 90 °C oven for another hour. The

resulting encapsulation thickness is $\sim$10 μm (Step 9 in Fig. 1). Because of capillary effect, the PDMS prepolymer sticks and rises along the sidewalls of the sacrificial posts. The combination of spin speed, spin duration, and baking conditions is designed to disperse the prepolymer to a film thickness less than the height of the sacrificial posts [26]. Additionally, the processing recipe guarantees that the prepolymer gets rid of the top of sacrificial posts [27], [28]. These conditions and the oxygen plasma pretreatment are crucial for successfully achieving the conical-well structure.

5) Opening Electrodes and Contact Pads: To remove sacrificial posts, the sample is immersed in acetone for about 10 min, and then, the electrode area is rinsed briefly with acetone stream. Confirmation that all electrodes have been opened can be achieved through microscope inspection; subsequent acetone soaking and rinsing are applied as necessary until all electrodes are opened (Step 10 in Fig. 1).

6) Detaching the Device From Glass Slide: The completed device is peeled off its glass slide, while immersed in isopropanol, which helps to reduce stress and prevent the film from self-adhesion (Step 11 in Fig. 1). Finally, the device is soaked in deionized water for 24 h to remove any chemical residues that may get involved during fabrication.

B. Device Characterization and Evaluation

1) Electrode Profile Characterization: In order to determine the dependence of conical well depth on sacrificial post height, three sets of samples were prepared. Within each set, one sample was made with the sacrificial layer spin coated at 400, 600, 700, 800, and 1000 r/min, respectively. The spin processes were all 30 s in duration with a ramp rate of 200 r/min/s. Subsequent processing parameters for the sacrificial layer, such as bake time, UV exposure dose, and development time, were adjusted according to the respective thickness. Other fabrication processes were kept the same. On each sample, two five-electrode MEAs were made. Therefore, data of 30 individual measurements on samples from three rounds of fabrication was collected for both post height and well depth at each spin speed. The profilometer (KLA-Tencor P15 Profilometer) settings in our measurements were: scan speed of 50 μm/s, sampling rate of 50 Hz, applied force of 0.5 mg, stylus tip radius of 2 μm with a 60° cone angle, and vertical range/resolution of 131 μm/0.0781 Å.

2) Electrode Impedance Measurement: To measure the electrode impedance, we used the same method and setup as were reported in [24]. The relationship between conical well depth (as determined by sacrificial layer spin speed) and electrode impedance was then quantified. One MEA with the sacrificial layer spin coated at 400, 600, 700, 800, and 1000 r/min, respectively, was tested. Five measurements of electrode impedance on the five individual electrodes of each MEA were taken. Because the PDMS surface is hydrophobic, when the MEA is immersed in water/solution or a solution drop is applied over the electrode area, an air bubble is usually trapped in each of the conical electrode wells, as shown in Fig. 5(a). This problem was prevented by brief oxygen plasma treatment to convert the PDMS surface to hydrophilic in advance [25]. The hydrophilicity lasted for more than one day in air (our observation), and can be preserved by storing the sample in deionized water [29].

3) Surface Contact Performance of Conical Wells: To test the performance of conical electrode wells when contacting to a surface in solution, an MEA (with its glass slide attached for ease of handling and observing) was immersed in deionized water in a Petri dish. A 25 $\times$ 25 $\times$ 0.2 mm glass slide (0.3 g) was placed over the electrodes. The conical wells were then inspected under an optical microscope.

4) Stimulation of In Vitro Spinal Cord: To evaluate the surface stimulation capability of the conical-well MEA, an *in vitro* preparation of isolated rat spinal cord was used [30]. Preparation of spinal cords was accomplished as detailed previously [31]. Viability of the spinal cord was confirmed prior to and throughout experimentation by observing evoked reflexes in the L2 ventral root following dorsal root L2 stimulation (using bipolar, glass suction stimulating, and recording electrodes). The degree of hindlimb-associated motor outputs elicited via MEA surface stimulation was compared to that evoked by a conventional rigid tungsten microelectrode. The conical-well MEA was wrapped around the spinal cord, such that its electrodes made continuous contact with the cord surface (see Fig. 6). Two-dimensional position of the stimulating electrode pair was mapped relative to pinned roots at T10 and T12 using a microscope grid eyepiece (resolution $<$ 50 μm; Leica). The comparison rigid tungsten microelectrode pair (5 μm tip diameter, 20–50 μm interelectrode distance, Harvard Apparatus, Inc., Holliston, MA) was pressed onto the cord surface at the same stimulus location either before or after MEA stimulation trials, using grid measurements for accurate placement. The MEA (through a custom-made electrode clamp) and the tungsten electrode pair were both connected to a multichannel stimulator (STG-2008, Multi Channel Systems). Single, rectangular current pulses (500 μA/50 μs) were applied to compare responses using the two different electrode types. A total of three isolated spinal cords were studied. For two of the spinal cords, an adjacent pair of MEA electrodes stimulated the dorsolateral funiculus (DLF) at thoracic levels 10 to 13. For the third spinal cord, an MEA electrode pair stimulated the ventrolateral funiculus (VLF) at thoracic level 12. Eight stimulus trials were conducted for each electrode type at a given site on the spinal cord surface. Evoked responses to spinal cord stimulation were recorded at vL2 and vL5 [32] (see Fig. 7) and analyzed using Clampfit (Molecular Systems) and customized MATLAB programs (Mathworks). The strengths of evoked responses [see Fig. 7(b) and (d)] were quantified by integrating the rectified response signal for 60 ms poststimulus artifact [see Fig. 7(a) and (c), yellow boxes] and subtracting from that value a rectified, prestimulus baseline value of equal duration.

III. Results

While the fabrication method can be adapted for customized MEAs with many electrodes, conical-well MEAs each of five electrodes (designed diameter 80 μm, minimum electrode spacing 230 μm) were fabricated (see Fig. 2) and used in experiments that characterized the electrode profile and electrode impedance,

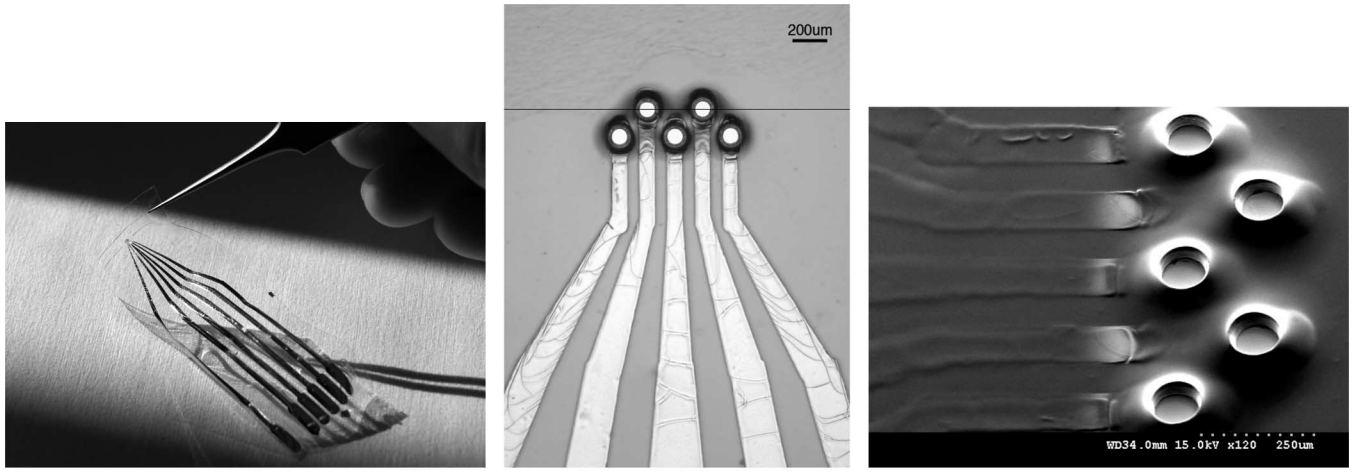

(a) (b) (c)

Fig. 2. Images of a five-electrode, conical-well MEA at different scales. The sacrificial layer of this sample was spin coated at 600 r/min. (a) MEA. (b) Optical microscope image of the conical-well microelectrodes. The dark line over the top two electrodes indicates the scanning track along which the conical-well microelectrode profiles in Fig. 3(a) were measured. (c) SEM image of the conical-well microelectrodes. The diameter of the electrodes was designed to be 80 μm. SEM measurements here show top and bottom diameters of $\sim$120 and $\sim$100 μm, respectively. The expansion of electrode size was caused primarily by PDMS shrinking as a result of release of embedded strains after removal of the sacrificial post in acetone.

and that evaluated the interfacing performance. The following sections describe these experimental results.

A. Electrode Profile Characterization

Our MEA features microelectrodes with a unique conical-well structure. To determine and measure the key fabrication parameters for such a structure, electrode profile was characterized as the sacrificial post height was varied. Sacrificial post height is important, because uncured PDMS prepolymer adheres to and rises along sidewall of the sacrificial post, and under the given processing conditions, a final height is achieved as a result of the balance between capillary force and gravity.

Fig. 3(a) shows a profilometer scan along the dark line in Fig. 2(b). Since the profilometer probe scanned from left to right, well depths were measured as the vertical distance between points A and B in Fig. 3(a). The inner wall of the well had a slightly conically recessed shape [see Figs. 2(c) and 3(a)]. This shape was created by the sacrificial post, which had a complementary, tapered shape due to nonuniform UV exposure dose through the thick photoresist layer [33] (Step 8 in Fig. 1). Such a particular shape provides an expected advantage of preventing the top edge of the well from bending inward into the well opening when making contact to a surface [see Fig. 5(b)].

However, in Fig. 3(a), the profilometer measurement is inaccurate in reflecting both the actual slope of the inner wall and the actual electrode opening diameter, due to the relatively large size of the probe and a possible shift of the scanning track from moving along the electrode diameter. SEM measurements showed that the actual electrode diameters were 20%–40% larger (depending on the depth of the well) than that was designed on the photomask, e.g., $\sim$100 μm instead of 80 μm for the sample in Fig. 2. This expansion of electrode size was caused primarily by PDMS shrinking as a result of release of embedded strains after removal of the sacrificial post in acetone.

The statistical dependence of conical well depth on sacrificial post height at different sacrificial layer spin speeds is shown in Fig. 3(b). Although there appear to be large deviations at some spin speeds, it was found during data analysis that both the post height and the electrode well depth were uniform across the five electrodes of each MEA, which is important for providing a consistent interfacial contact. Generally, a conical well depth at the value of about one electrode radius is found to have the best overall performance [34], [35].

B. Electrode Impedance Measurement

Fig. 4 shows the average electrode impedance curves corresponding to each sacrificial layer spin speed, and Table I gives the average impedance values at 1 kHz. It is seen that, at most frequencies, the electrode impedance is higher when the spin speed is lower. Slower spin speed results in thicker sacrificial layer, which subsequently results in more significantly tapered sacrificial posts due to nonuniform UV exposure dose through the photoresist layer. Consequently, slower spin speed, which ultimately results in a smaller actual electrode opening area and a deeper electrode well, was shown to correspond to higher electrode impedance. This is because electrode impedance is inversely correlated to the actual electrode opening area and directly correlated to parasitic impedances potentially building up on the inner wall of the electrode well.

The results in Fig. 4 and Table I, on the whole, confirm the expected relationship between sacrifical layer thickness and electrode impedance. However, slight mismatches do exist; potential reasons for these deviations include variations in electrode surface roughness between certain electrodes, as well as the degree of presence of residues on certain electrode surfaces. Also, for sacrificial layers of close thicknesses, like those resulted from 800 and 1000 r/min spins, the tapered effects were not strictly in a descending order due to potential UV over- or underexposure. Therefore, some of the actual electrode opening areas deviated

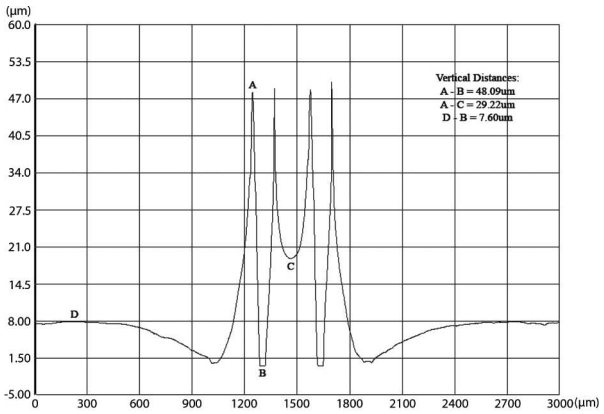

Fig. 3. Characterization of conical-well microelectrode profile. (a) Profilometer scan along the dark line in Fig. 2(b). The sacrificial layer of this sample was spin coated at 400 r/min. Well depth was measured as the vertical distance between points A and B. (b) Statistical dependence of conical well depth on sacrificial post height at different sacrificial layer spin speeds. Each point on the plot corresponds to measurements on 30 individual electrodes from three rounds of fabrication. Each group of data is fitted by a second-order polynomial curve (the dotted line).

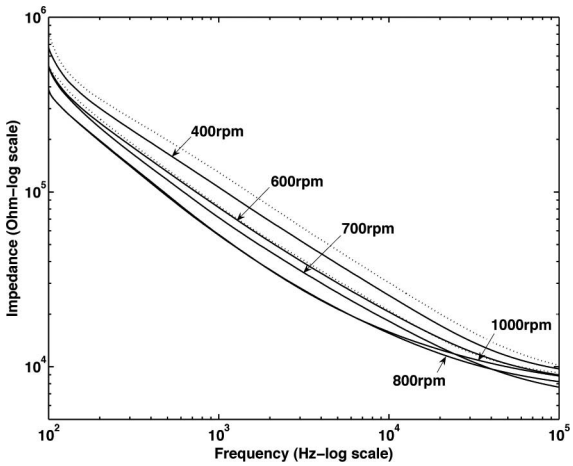

Fig. 4. Electrode impedance measurement. Average electrode impedance curves corresponding to each sacrificial layer spin speed are shown. Curves with one standard deviation from the average electrode impedance corresponding to a sacrificial layer spin coated at 400 r/min are also shown as dotted lines.

TABLE 1
AVERAGE ELECTRODE IMPEDANCES AT 1 KHZ CORRESPONDING TO EACH SACRIFICIAL LAYER SPIN SPEED (IMPEDANCE UNIT: KΩ)

	400rpm	600rpm	700rpm	800rpm	1000rpm
1kHz	106.44	81.538	71.405	56.632	57.072

from the normal trend, causing mismatches in the statistical results.

Fig. 4 together with Table I indicates that the electrode impedances compare favorably to those of rigid-substrate MEA electrodes [10], [11], [36], and are relatively uniform across electrodes.

C. Surface Contact Performance of Conical Wells

Fig. 5(b) shows the interfacial contact between the conical electrode wells and a thin glass slide. It can be seen that each electrode well forms a perfect seal (the light rings surrounding each electrode) on the glass surface, without any inward bending. Moreover, it was observed that when the thin glass slide was initiated a slight displacement with respect to the MEA, the electrode wells still sealed to the original sites, despite being stretched to irregular shapes (image not shown). As a result of the conformability and elasticity of PDMS material combined with the special structure of the electrode well, it is also expected that, in a similar manner, the conical-well electrode can potentially create a highly isolated microenvironment on the neural tissue surface, which could improve the efficacy of electrical current exchange during neural interfacing.

D. Stimulation of In Vitro Spinal Cord

Our preliminary comparisons of the MEA versus rigid tungsten microelectrode demonstrate that the MEA is similar to rigid tungsten microelectrodes in its ability to evoke ventral root outputs via spinal cord surface stimulation (see Fig. 7). When placed on T12 DLF ($n = 2$), the MEA and rigid tungsten microelectrode evoked vL2 responses with similar strengths [data for one of two spinal cords shown in Fig. 7(a) and (b)]. Also similarly, both electrode types evoked little to no response at vL5. The MEA, when placed at T12 VLF ($n = 1$), evoked ventral root vL2 and vL5 responses with similar shape and timing characteristics as responses evoked by the rigid tungsten microelectrode (Fig. 7(c), indicated by arrows). However, the strength of evoked vL2 and vL5 responses was greater for the MEA than for the rigid tungsten microelectrode [see Fig. 7(d)]. Together, these results from stimulating with the MEA and rigid tungsten microelectrode at these two physiologically relevant spinal cord sites [37]–[42] demonstrate that the MEA is capable of eliciting motor outputs in a similar manner to traditional rigid electrodes, and confirm the suitability of the MEA for use in future surface stimulation studies in spinal cord.

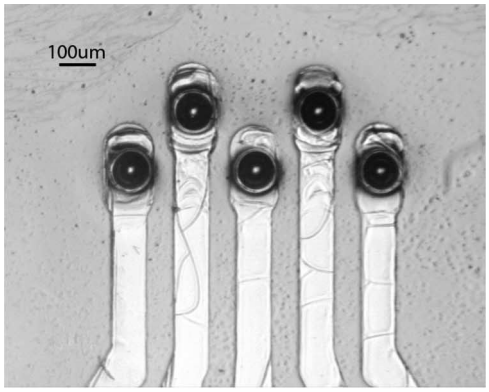

(a)

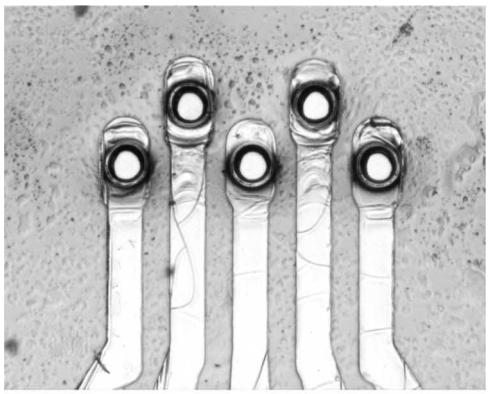

(b)

Fig. 5. Optical microscope images for surface contact performance of conical electrode wells. (a) MEA with its glass slide attached for ease of handling and observing was immersed in deionized water in a Petri dish. An air bubble was trapped in each of the conical electrode wells due to hydrophobicity of the PDMS surface. These bubbles can be avoided by brief oxygen plasma activation of the PDMS surface in advance. (b) Interfacial contact between conical electrode wells and a thin glass slide placed over. Air bubbles were avoided. Each electrode well formed a good seal (the light rings surrounding each electrode) on the glass surface, without any inward bending.

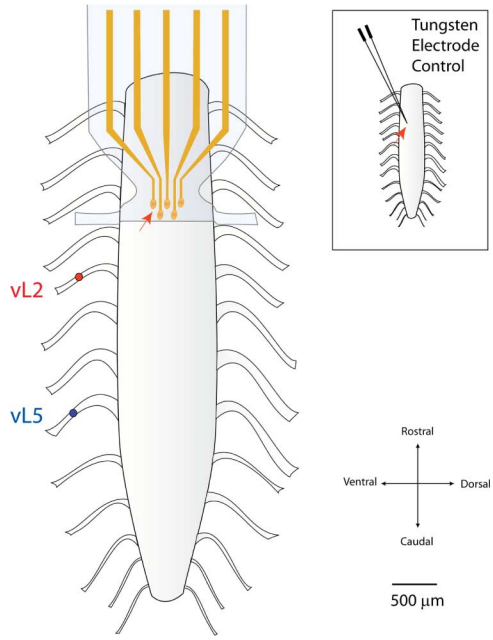

Fig. 6. Experimental setup for comparing spinal cord responses to surface stimulation with the conical-well MEA versus rigid tungsten electrode. Studies were performed to determine the capability of the conical-well MEA to access motor circuitry in the *in vitro* rat isolated spinal cord, as compared to a rigid tungsten microelectrode (inset, placed on location immediately between the two leftmost MEA electrodes, location indicated by arrows). Single-pulse stimuli were delivered to the surface of the cord and motor output responses were recorded at ventral roots L2 (vL2, red) and L5 (vL5, blue).

IV. Discussion

A. Fabrication Considerations

Our fabrication method has demonstrated the achievement of PDMS-based MEAs with conical-well microelectrodes for improved surface contact. Moreover, it is a clean process in that no metal wet etching is involved, thus no etchant residue is potentially left in the device. Preliminary results showed that our fabrication method could achieve a single electrode with minimum diameter of $\sim$10 μm, a 10 $\times$ 10 electrode array with minimum electrode diameter of 20 μm (60 μm center–center electrode distance), and a single trace with thinnest width of 10 μm. Some thoughts with regard to our fabrication method are discussed in the following.

1) Method for Patterning Gold Features: Many methods have previously been explored for patterning metal films on PDMS substrate, including using shadow masking [22], laser cutting [23], metal transfer [43], wet etching [24], and liftoff [21], [28]. We have chosen the liftoff method for its high resolution, flexibility on pattern design, as well as process compatibility and cleanness. However, liftoff on PDMS substrate is much harder than on a rigid substrate like silicon or glass, primarily due to its large coefficient of thermal expansion (CTE, $\sim$310 ppm/°C [44]). Additionally, most stripping liquids, like acetone, used in rigid-substrate liftoff processes are not compatible with PDMS substrate, because they can easily deform the substrate and liftoff all desired features. Thus, most negative photoresists are not suitable in our process due to their difficulty in stripping after development without using solvents, with the exception that a compatible stripper exists (e.g., RR4 or RR41 from Futurrex for its NR series, as has been used in [27]). Considering these, we focused on developing an efficient, high-resolution liftoff method using a positive photoresist with its developer as the stripper.

The positive photoresist we finally chose (Shipley Megaposit SPR 220 7.0) can produce robust high-resolution features and adheres strongly to the activated PDMS surface: although a few cracks may develop after baking, no pieces come off during processing. Most other photoresists, including both positive and negative, do not adhere to the PDMS substrate strongly enough; as a result, small cracked pieces drop off during development. Additionally, the lack of a strong adhesion of these other photoresists to PDMS substrate results in small photoresist features being lifted off the PDMS substrate during development.

The thickness of the photoresist mask is also very important for an efficient and complete liftoff. We have determined that a 12 μm layer is optimal for achieving liftoff with feature sizes no smaller than 10 μm. The SPR 220 7.0 mask layer can be easily dissolved by the mild developer MF-319, with the condition

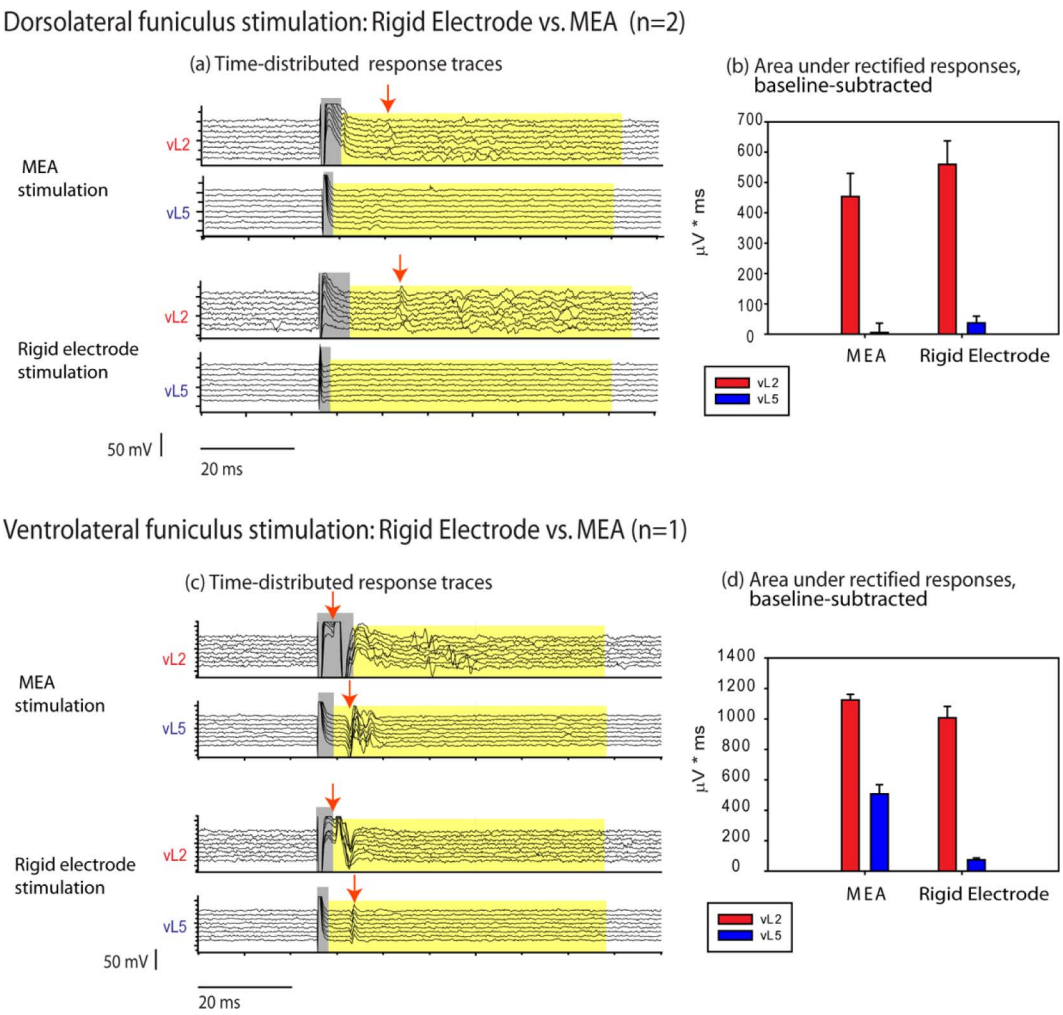

Fig. 7. Ventral root responses to surface stimulation of the spinal cord, rigid electrode versus MEA. A pair of MEA electrodes (bipolar configuration) and a rigid bipolar tungsten electrode were used to stimulate the spinal cord at surface sites on thoracic level 12 (T12) DLF and VLF ($n = 3$ cords). A microscope grid eyepiece was used to measure and replicate surface positional coordinates across electrode types. Shown are ventral root L2 (vL2) and ventral root L5 (vL5) responses to MEA and rigid electrode stimulation at T12 DLF [(a), data from 1 of 2 cords shown] and T12 VLF [see (c)]. Eight stimulus trials were conducted per electrode type; these response traces are shown time distributed. The strength of evoked responses was quantified by integrating the rectified response signal (poststimulus artifact) and subtracting from that value a rectified, prestimulus baseline of equal duration [60 ms; (b) and (d)]. Standard error bars are shown. Time windows during which stimulus artifact was observed (indicated by gray boxes) were not included in the time range over which strengths of response were measured (yellow boxes). Initial ventral root responses to stimuli can be observed within and after the stimulus artifact (as indicated by arrows), which indicates that stimulus artifact presents a limitation to the accuracy of the strength-of-response calculations. Ventral root L2 (vL2) responses to DLF stimulation were similar in strength for both electrodes, and vL5 responses were similarly small or undetectable using both electrode types [see (b)]. For VLF stimulation, the pattern of vL2 and vL5 responses was similar across electrode types, with larger responses evoked at L2 [see (d)]. At the T12 VLF, stronger responses were evoked on both vL2 and vL5 for MEA stimulation versus rigid electrode stimulation.

that it should be flood-exposed before depositing metal film on. Also, MF-319 is compatible and clean for the process.

2) Acetone Effects on PDMS: It was interesting that while we found acetone could not be used for stripping in our liftoff process (because it deformed the PDMS substrate and caused gold features to be stripped off), we could use it to remove sacrificial posts for opening electrodes and contact pads. Our encapsulated devices were found robust enough to withstand being soaked in acetone for an hour during sacrificial post removal! It was believed that the surface properties of PDMS in the encapsulated device changed following our processing, which made it harder for acetone to get into the polymer. Nevertheless, PDMS thin films are not suitable to be soaked in acetone for too long. About an hour would be the maximal limit, and longer immersion may cause PDMS to be "dissolved" by acetone.

3) Sacrificial Posts for Opening Electrodes and Contact Pads: The selection of a suitable photoresist for making sacrificial posts depended on several key factors. The associated processing of the chosen photoresist needed to be compatible with the PDMS substrate and previous processes. Also, the chosen photoresist needed to be PDMS-philic (after oxygen plasma activation) for the formation of electrode wells and capable of producing features with superior resolution and aspect ratio. Finally, the photoresist needed to be removable with a compatible process in the end. After exploration, we finally found the negative photoresist NR5-8000 (Futurrex, Inc.) could meet

all the aforementioned requirements. Results also show that, with proper process parameters, planar electrodes could be fabricated [27], [28], [45].

B. Advantages of Conical-Well Electrodes

The major perceived advantage of the conical-well electrode is its potential to provide an optimal functional interface with soft tissue. Evidences of this potential are explained in detail in the following, and are described in relation to our investigations concerning the physical, electrical, and mechanical attributes of such MEAs.

1) Providing Good Suction Interface for Surface Contact: As demonstrated in Section III-C, when contacting to a flat glass surface, the conical electrode wells each formed a tight seal. In a similar manner, it is expected that conical-well microelectrodes, when interfaced with soft tissues, would provide an interface with a more isolated microenvironment for current exchange between the electrode and tissue surface. With this seal, little current leakage should occur, and stimulation would be more power efficient with improved spatial selectivity. However, more sophisticated experiments need to be designed to further investigate such a potential.

2) Producing Uniform Current Density Profile: For near-field electrical stimulation, in which the targeted tissue is immediately adjacent to or in direct contact with the electrode surface, charge density (the product of current density and pulse duration), together with charge per phase, is considered responsible for stimulation induced neural damage [46]. Excess current density at the electrode surface can also cause electrode damage by initiating irreversible electrochemical reactions. Safe stimulation levels are thus set by limiting the maximum average current density at the electrode surface and the maximum average charge injection into the tissue per phase.

For nonrecessed disk electrodes, peak current density builds up at electrode–insulator edges [47]. Theoretical analyses [34] and experimental measurements [35] have demonstrated that excess current density at the electrode edges can be reduced or eliminated by recessing the electrode into the carrier, creating a welled electrode, and by radially varying the recess. Thus, recessed electrodes could significantly reduce tissue damage by preventing the electrode surface from irreversible electrochemical reactions and by protecting the targeted tissue from being exposed to high-peak current density.

Our conical-well electrode features a conical recess, which is molded by a tapered sacrificial post. The recess slope can be set by controlling sidewall slope of the sacrificial post [45], and the recess depth can be set by controlling height of the sacrificial post [see Fig. 3(b)]. Uniform distributions of current density are expected at both the electrode surface and the conical-well aperture, where interface junction is to be made with targeted tissue surface [35]. Not only will current be released uniformly across the electrode surface, thereby minimizing electrode damage, but also the maximum amount of current can be injected uniformly across the conical-well aperture into the targeted tissue, thus maximizing activation capability, while minimizing direct tissue damage normally caused by edge-induced excess peak current density.

3) Protecting Electrodeposited Material: Previous work has demonstrated that platinum black [48], [49], iridium oxide [50], and conducting polymers [51], [52] can be electrodeposited onto electrode surface. Such electrodeposition benefits electrode designs by reducing electrode impedance and increasing charge injection capability. The conical-well structure is expected to facilitate such electrodepositing efforts by protecting the deposited material from mechanical removal. However, the deposited rough material in the well could disturb the uniformity of current density distributions. Therefore, a tradeoff between electrode impedance reduction, charge injection increase, and current density uniformity must be optimized. This can be accomplished by appropriate control of material deposition and by adjusting the conical-well profile with respect to well depth and recess slope.

C. Potential Applications

This PDMS-based conformable MEA technology could benefit numerous applications that require conformable device contact with biological tissue surfaces and minimal tissue damage that often results from rigid electrodes. For example, the fabrication method we have developed has the potential for producing efficient interfaces for high-resolution prostheses on the surface of the retina, cortex, and spinal cord: applications in which conformable thin-film MEAs of high capacity and high-electrode density are desired. Most electrical stimulation applications would benefit from the conical-well electrode feature, because its uniform current density profile provides the advantage of minimal tissue damage and electrode corrosion; this advantage is particularly important for chronic stimulation applications. For recording applications, the conical wells have the potential to facilitate better-isolated electrodes, thus reducing leakage and noise and increasing signal fidelity.

Although we have used compliant PDMS (Sylgard 184, Dow Corning) as both the substrate and encapsulation materials and have used gold to make the interconnects, the fabrication technique also has the potential for implementing conical-well MEAs on other substrates, either rigid or flexible, and with other metals or conducting polymers used for the interconnects. The advantages of conical-well MEAs fabricated using other materials would open the technology to a broader range of applications. For example, silicon, glass, or polyimide can be used for the substrate, and SU-8, polyimide or PDMS can be used for encapsulation; the resulting planar devices would have applicability to *in vitro* applications—such as brain-slice studies—in which the uniform current density profile and potentially higher signal fidelity of the conical wells can be exploited.

ACKNOWLEDGMENT

The authors would like to thank E. Brown and Dr. J. Ross for providing valuable suggestions through discussions.

REFERENCES

[1] K. C. Cheung, "Implantable microscale neural interfaces," *Biomed. Microdevices*, vol. 9, pp. 923–938, 2007.

[2] K. D. Wise, J. B. Angell, and A. Starr, "An integrated circuit approach to extracellular microelectrodes," *IEEE Trans. Biomed. Eng.*, vol. BME-17, no. 3, pp. 238–247, Jul. 1970.

[3] K. D. Wise and J. B. Angell, "A low-capacitance multielectrode probe for neurophysiology," *IEEE Trans. Biomed. Eng.*, vol. BME-22, no. 3, pp. 212–219, May 1975.

[4] B. Qing and K. D. Wise, "Single-unit neural recording with active microelectrode arrays," *IEEE Trans. Biomed. Eng.*, vol. 48, no. 8, pp. 911–920, Aug. 2001.

[5] P. K. Campbell, K. E. Jones, R. J. Huber, K. W. Horch, and R. A. Normann, "A silicon-based, three-dimensional neural interface: manufacturing processes for an intracortical electrode array," *IEEE Trans. Biomed. Eng.*, vol. 38, no. 8, pp. 758–768, Aug. 1991.

[6] K. E. Jones, P. K. Campbell, and R. A. Normann, "A glass/silicon composite intracortical electrode array," *Ann. Biomed. Eng.*, vol. 20, pp. 423–437, 1992.

[7] M. A. Nicolelis, A. A. Ghazanfar, C. R. Stambaugh, L. M. Oliveira, M. Laubach, J. K. Chapin, R. J. Nelson, and J. H. Kaas, "Simultaneous encoding of tactile information by three primate cortical areas," *Nat. Neurosci.*, vol. 1, no. 7, pp. 621–630, 1998.

[8] G. W. Gross, "Simultaneous single unit recording in vitro with a photoetched laser deinsulated gold multimicroelectrode surface," *IEEE Trans. Biomed. Eng.*, vol. BME-26, no. 5, pp. 273–279, May 1979.

[9] J. Pine, "Recording action potentials from cultured neurons with extracellular microcircuit electrodes," *J. Neurosci. Methods*, vol. 2, no. 1, pp. 19–31, 1980.

[10] H. Oka, K. Shimono, R. Ogawa, H. Sugihara, and M. Taketani, "A new planar multielectrode array for extracellular recording: application to hippocampal acute slice," *J. Neurosci. Methods*, vol. 93, no. 1, pp. 61–67, 1999.

[11] M. O. Heuschkel, M. Fejtl, M. Raggenbass, D. Bertrand, and P. Renaud, "A three-dimensional multi-electrode array for multi-site stimulation and recording in acute brain slices," *J. Neurosci. Methods*, vol. 114, no. 2, pp. 135–148, 2002.

[12] D. A. Wagenaar, J. Pine, and S. M. Potter, "Effective parameters for stimulation of dissociated effective parameters for stimulation of dissociated cultures using multi-electrode arrays," *J. Neurosci. Methods*, vol. 138, pp. 27–37, 2004.

[13] P. J. Rousche, D. S. Pellinen, D. P. Pivin, J. C. Williams, R. J. Vetter, and D. R. Kipke, "Flexible polyimide-based intracortical electrode arrays with bioactive capability," *IEEE Trans. Biomed. Eng.*, vol. 48, no. 3, pp. 361–371, Mar. 2001.

[14] C. Gonzalez and M. Rodriguez, "A flexible perforated microelectrode array probe for action potential recording in nerve and muscle tissues," *J. Neurosci. Methods*, vol. 72, no. 2, pp. 189–195, Apr. 1997.

[15] T. Stieglitz, H. Beutel, C. Blau, and J. U. Meyer, "Flexible multichannel microelectrodes with integrated leads for use in neuroprosthetics," in *Proc. Biomed. Tech. (Berl)*, 1997, vol. 42, pp. 449–450.

[16] B. G. Lapatki, J. V. Dijk, I. E. Jonas, M. J. Zwarts, and D. F. Stegeman, "A thin, flexible multielectrode grid for high-density surface EMG," *J. Appl. Physiol.*, vol. 96, no. 1, pp. 327–336, Jan. 2004.

[17] S. A. Boppart, B. C. Wheeler, and C. S. Wallace, "A flexible perforated microelectrode array for extended neural recordings," *IEEE Trans. Biomed. Eng.*, vol. 39, no. 1, pp. 37–42, Jan. 1992.

[18] J. F. Rizzo, J. L. Wyatt, J. Loewenstein, S. Kelly, and D. Shire, "Perceptual efficacy of electrical stimulation of human retina with a microelectrode array during short-term surgical trials," *Invest Ophthalmol. Vis. Sci.*, vol. 44, no. 12, pp. 5362–5369, Dec. 2003.

[19] J. F. Rizzo, J. L. Wyatt, J. Loewenstein, S. Kelly, and D. Shire, "Methods and perceptual thresholds for short-term electrical stimulation of human retina with microelectrode arrays," *Invest Ophthalmol. Vis. Sci.*, vol. 44, no. 12, pp. 5355–5361, Dec. 2003.

[20] S. Takeuchi and I. Shimoyama, "A radio-telemetry system with a shape memory alloy microelectrode for neural recording of freely moving insects," *IEEE Trans. Biomed. Eng.*, vol. 51, no. 1, pp. 133–137, Jan. 2004.

[21] M. Maghribi, J. Hamilton, D. Polla, K. Rose, T. Wilson, and P. Krulevitch, "Stretchable micro-electrode array [for retinal prosthesis]," in *Proc. 2nd Annu. Int. IEEE-EMB Spec. Topic Conf. Microtechnol. Med. Biol.*, May, 2002, pp. 80–83.

[22] S. P. Lacour, C. Tsay, S. Wagner, Z. Yu, and B. Morrison, "Stretchable micro-electrode arrays for dynamic neuronal recording of in vitro mechanically injured brain," in *Proc. 4th IEEE Conf. Sens.*, 2005, pp. 617–620.

[23] M. Schuettler, S. Stiess, B. V. King, and G. J. Suaning, "Fabrication of implantable microelectrode arrays by laser cutting of silicone rubber and platinum foil," *J. Neural Eng.*, vol. 2, pp. S121–S128, 2005.

[24] K. W. Meacham, R. J. Giuly, L. Guo, S. Hochman, and S. P. DeWeerth, "A lithographically-patterned, elastic multi-electrode array for surface stimulation of the spinal cord," *Biomed. Microdevices*, vol. 10, no. 2, pp. 259–269, Apr. 2008.

[25] B. H. Jo, L. V. Lerberghe, K. M. Motsegood, and D. J. Beebe, "Three-dimensional micro-channel fabrication in polydimethylsiloxane (PDMS) elastomer," *J. Microelectromech. Syst.*, vol. 9, no. 1, pp. 76–81, 2000.

[26] D. C. Duffy, R. J. Jackman, K. M. Vaeth, K. F. Jensen, and G. M. Whitesides, "Patterning electroluminescent materials with feature sizes as small as 5 μm using elastomeric membranes as masks for dry lift-off," *Adv. Mater.*, vol. 11, no. 7, pp. 546–552, 1999.

[27] J. Park, H. S. Kim, and A. Han, "Micropatterning of poly(dimethylsiloxane) using a photoresist lift-off technique for selective electrical insulation of microelectrode arrays," *J. Micromech. Microeng.*, vol. 19, no. 6, p. 065016, May 2009.

[28] M. A. McClain, M. C. LaPlaca, and M. G. Allen, "Spun-cast micromolding for etchless micropatterning of electrically functional PDMS structures," *J. Micromech. Microeng.*, vol. 19, no. 10, pp. 107002-1–107002-6, Sep. 2009.

[29] J. C. McDonald and G. M. Whitesides, "Poly(dimethylsiloxane) as a material for fabricating microfluidic devices," *Acc. Chem. Res.*, vol. 35, no. 7, pp. 491–499, 2002.

[30] S. Hochman and B. J. Schmidt, "Whole cell recordings of lumbar motoneurons during locomotor-like activity in the in vitro neonatal rat spinal cord," *J. Neurophysiol.*, vol. 79, no. 2, pp. 743–752, Feb. 1998.

[31] B. L. Shay, M. Sawchuk, D. W. Machacek, and S. Hochman, "Serotonin 5-ht2 receptors induce a long-lasting facilitation of spinal reflexes independent of ionotropic receptor activity," *J. Neurophysiol.*, vol. 94, no. 4, pp. 2867–2877, 2005.

[32] O. Kiehn and O. Kjaerulff, "Spatiotemporal characteristics of 5-ht and dopamine-induced rhythmic hindlimb activity in the in vitro neonatal rat," *J. Neurophysiol.*, vol. 75, no. 4, pp. 1472–1482, 1996.

[33] K. Kim, D. S. Park, H. M. Lu, W. Che, K. Kim, J.-B. Lee, and C. H. Ahn, "A tapered hollow metallic microneedle array using backside exposure of su-8," *J. Micromech. Microeng.*, vol. 14, pp. 597–603, 2004.

[34] J. T. Rubinstein, F. A. Spelman, M. Soma, and M. F. Suesserman, "Current density profiles of surface mounted and recessed electrodes for neural prostheses," *IEEE Trans. Biomed. Eng.*, vol. BME-34, no. 11, pp. 864–875, Nov. 1987.

[35] M. F. Suesserman, F. A. Spelman, and J. T. Rubinstein, "In vitro measurement and characterization of current density profiles produced by nonrecessed, simple recessed, and radially varying recessed stimulating electrodes," *IEEE Trans. Biomed. Eng.*, vol. 38, no. 5, pp. 401–408, May 1991.

[36] A. K. Ahuja, M. R. Behrend, J. J. Whalen, M. S. Humayun, and J. D. Weiland, "The dependence of spectral impedance on disc microelectrode radius," *IEEE Trans. Biomed. Eng.*, vol. 55, no. 4, pp. 1457–1460, Apr. 2008.

[37] T. Iwahara, Y. Atsuta, E. Garcia-Rill, and R. D. Skinner, "Spinal cord stimulation-induced locomotion in the adult cat," *Brain Res. Bull.*, vol. 28, no. 1, pp. 99–105, 1992.

[38] D. S. Magnuson and T. C. Trinder, "Locomotor rhythm evoked by ventrolateral funiculus stimulation in the neonatal rat spinal cord in vitro," *J. Neurophysiol.*, vol. 77, no. 1, pp. 200–206, 1997.

[39] M. R. Dimitrijevic, Y. Gerasimenko, and M. M. Pinter, "Evidence for a spinal central pattern generator in humans," *Ann. N. Y. Acad. Sci.*, vol. 860, pp. 360–376, 1998.

[40] Y. P. Gerasimenko, I. A. Lavrov, I. N. Bogacheva, N. A. Shcherbakova, V. I. Kucher, and P. E. Musienko, "Formation of locomotor patterns in decerebrate cats in conditions of epidural stimulation of the spinal cord," *Neurosci. Behav. Physiol.*, vol. 35, no. 3, pp. 291–298, 2005.

[41] R. M. Ichiyama, Y. P. Gerasimenko, H. Zhong, R. R. Roy, and V. R. Edgerton, "Hindlimb stepping movements in complete spinal rats induced by epidural spinal cord stimulation," *Neurosci. Lett.*, vol. 383, no. 3, pp. 339–344, 2005.

[42] D. Barthélemy, H. Leblond, J. Provencher, and S. Rossignol, "Nonlocomotor and locomotor hindlimb responses evoked by electrical microstimulation of the lumbar cord in spinalized cats," *J. Neurophysiol.*, vol. 96, no. 6, pp. 3273–3292, 2006.

[43] D. S. Gray, J. Tien, and C. S. Chen, "High-conductivity elastomeric electronics," *Adv. Mater.*, vol. 16, no. 5, pp. 393–397, 2004.

[44] M. V. Kunnavakkam, F. M. Houlihan, M. Schlax, J. A. Liddle, P. Kolodner, O. Nalamasu, and J. A. Rogers, "Low-cost, low-loss microlens arrays fabricated by soft-lithography replication process," *Appl. Phys. Lett.*, vol. 82, no. 8, pp. 1152–1154, 2003.
[45] L. Guo and S. P. DeWeerth, "PDMS-based conformable microelectrode arrays with selectable novel 3-D microelectrode geometries for surface stimulation and recording," in *Proc. IEEE Eng. Med. Biol. Soc. 31st Ann. Int. Conf.*, Minneapolis, MN, Sep. 2–6, 2009.
[46] D. B. McCreery, W. F. Agnew, T. G. Yuen, and L. Bullara, "Charge density and charge per phase as cofactors in neural injury induced by electrical stimulation," *IEEE Trans. Biomed. Eng.*, vol. 37, no. 10, pp. 996–1001, Oct. 1990.
[47] J. Newman, "Current distribution on a rotating disk below the limiting current," *J. Electrochem. Soc.*, vol. 113, pp. 1235–1241, Dec. 1966.
[48] D. A. Borkholder, "Cell based biosensors using microelectrodes," Ph.D. dissertation, Stanford Univ., Stanford, CA, 1998.
[49] W. Franks, W. Schenker, P. Schmutz, and A. Hierlemann, "Impedance characterization and modeling of electrodes for biomedical applications," *IEEE Trans. Biomed. Eng.*, vol. 52, no. 7, pp. 1295–1302, Jul. 2005.
[50] R. D. Meyer, S. F. Cogan, T. H. Nguyen, and R. D. Rauh, "Electrodeposited iridium oxide for neural stimulation and recording electrodes," *IEEE Trans. Neural Syst. Rehab. Eng.*, vol. 9, no. 1, pp. 2–11, Mar. 2001.
[51] X. Cui, J. F. Hetke, J. A. Wiler, D. J. Anderson, and D. C. Martin, "Electrochemical deposition and characterization of conducting polymer polypyrrole/pss on multichannel neural probes," *Sens. Actuators A*, vol. 93, pp. 8–18, 2001.
[52] X. Cui and D. C. Martin, "Fuzzy gold electrodes for lowering impedance and improving adhesion with electrodeposited conducting polymer films," *Sens. Actuators A*, vol. 103, pp. 384–394, 2003.

Liang Guo (S'07) received the B.S. degree in biomedical engineering from Tsinghua University, Beijing, China, in 2004. He is currently working toward the Ph.D. degree in the bioengineering program from Georgia Institute of Technology, Atlanta, GA.

His current research interests include neural interfacing technology, including microelectrode arrays, simultaneous recording and stimulation, circuits, signal processing, and prostheses.

Mr. Guo is a Student Member of the Engineering in Medicine and Biology Society, the Society for Neuroscience, and the Materials Research Society. He is also a Full Member of Sigma Xi.

Kathleen W. Meacham (S'06) received the B.S. degree in electrical and computer engineering from Carnegie Mellon University, Pittsburgh, PA, in 2001, and the Ph.D. degree in biomedical engineering from Georgia Institute of Technology and Emory University, Atlanta, GA, in 2008. She is currently working toward the M.D. degree from Emory University School of Medicine, Atlanta.

Her current research interests include translating medical device development into improved therapeutic approaches.

Dr. Meacham is also a member of the Engineering in Medicine and Biology Society, the Society for Neuroscience, and the American Medical Student Association.

Shawn Hochman received the B.S. degree in zoology and the Ph.D. degree in physiology from the University of Manitoba, Winnipeg, MB, Canada, in 1983 and 1989, respectively.

He is currently an Associate Professor in physiology at Emory University School of Medicine, Atlanta, GA, where he is also a Program Faculty member in neuroscience. He is also a Program Faculty member in biomedical engineering at Emory/Georgia Institute of Technology, Atlanta. His research interests include electrophysiological plasticity of spinal cord functional systems.

Dr. Hochman is a member of the American Association for the Advancement of Science, the Society for Neuroscience, and the American Physiological Society.

Stephen P. DeWeerth (S'85–M'90–SM'03) received the M.S. degree in computer science and the Ph.D. degree in computation and neural systems from California Institute of Technology, Pasadena, CA, in 1987 and 1991, respectively.

He is currently a Professor in the Wallace H. Coulter Department of Biomedical Engineering and in the School of Electrical and Computer Engineering, Georgia Institute of Technology, Atlanta, GA, and at the Emory University School of Medicine, Atlanta. His research interests include the implementation of neuromorphic electronic and robotic systems, the development of neural interfacing technologies, and the study of the biological control of movement.